

Cubic to hexagonal iron phase transition promoted by interstitial hydrogen

A. Castedo,¹ J. Sanchez,¹ J. Fullea,² M.C. Andrade,² and P.L. de Andres ^{*3}

¹ *Instituto de Ciencias de la Construcción Eduardo Torroja, IETcc-CSIC, Madrid (Spain)*

² *Centro de Seguridad y Durabilidad Estructural y de Materiales, CISDEM-UPM-CSIC, Madrid (Spain)*

³ *Donostia International Physics Center (DIPC), Paseo Manuel Lardizabal 4, 20018 San Sebastian (Spain)*

(Dated: May 25, 2022)

Abstract

Using ab-initio density functional theory we study the role of interstitial hydrogen on the energetics of the phase transformation of iron from bcc to hcp along Bain's pathway. The impurity creates an internal stress field that can be released through a tetragonal distortion of the lattice, promoting the bcc (ferromagnetic) \rightarrow fcc (frustrated antiferromagnetic) \rightarrow hcp (ferromagnetic) transition. The transformation between crystal systems is accompanied by a drastic magnetic reorganization and sudden variations of the unit cell volume, that can be one of the reasons for embrittlement and mechanical failure of iron upon hydrogen adsorption.

PACS numbers: 62.20.mj, 64.70.K-, 66.30.J-, 81.30.Kf

Keywords: iron, hydrogen, interstitial, bcc (α -iron), fcc (γ -iron), hcp (ϵ -iron), fragilization, embrittlement, ab-initio, density functional, phase transition

* On leave of absence from Instituto de Ciencia de Materiales de Madrid (CSIC) 28049 Madrid (Spain)

Introduction. Interstitial impurities play a key role on mechanical and structural properties of different metals. In particular, interstitial hydrogen has been identified as a promoter of mechanical failure under stress; a point of particular interest in the technological areas of engineering and construction. These processes, known by the generic name of embrittlement, are subject to active research in the field of high-strength steels, of which the primary component is ferromagnetic body-centered cubic iron (bcc, also referred as α -iron). [1–6] Furthermore, hydrogen dissolved in iron at very high pressures is fundamental to understand the behavior of the Earth’s core, in particular the long-standing controversy about its density and even its crystalline phase.[7, 8] Experimental information in these areas is difficult to obtain and sometimes contradictory. Therefore, a key element to make progress in such complex but fundamental problems is the use of accurate ab-initio density functional theory (DFT), that can provide guiding in the interpretation and new motivation for gathering further experimental evidence.

In the cubic lattice there are two high-symmetry sites competing to host interstitial impurities: the tetrahedral and octahedral sites. Absorption in the octahedral site creates an anisotropic stress field that favors a tetragonal distortion, making the bcc configuration unstable and driving the unit cell towards a phase transition to a face-centered cubic lattice (fcc) first, and then an hexagonal one (hcp). Absorption on the tetrahedral site, on the other hand, results in a more isotropic stress distribution and merely provokes an increase of the volume. There has been an ongoing controversy in the literature about the actual absorption site for interstitial hydrogen in ferromagnetic bcc iron. This is partly related to the fact that the two competing available high-symmetry sites are very similar in energy, making difficult to accurately decide between them because of the many different factors involved. In particular, as the computed energy difference between them is similar to $k_B T$ at room temperature, an equilibrium distribution between both sites should exist. Furthermore, external stresses can contribute to the energy enough to influence that distribution, and a many-body contribution depending on the interstitials density can influence the final distribution. Currently accepted wisdom takes the tetrahedral site (T) as the most likely absorption site for the low-temperature, low-density phase, while the octahedral site (O) is preferred for large concentrations of interstitials.[9–11] From a physical point of view, this is related to the internal stress originated from the occupation of O-sites, causing a tetragonal distortion of the bcc lattice and making unfavorable the occupation of T-sites for

large densities of interstitials. Generally speaking, overall hydrogen solubility in bcc iron is low, favoring the occupancy of T-sites. However, occupation of O-sites cannot be neglected under some circumstances, e.g.: (i) if there is a local accumulation of interstitial hydrogen, e.g. due to preferential nucleation near defects, which would keep solubility low over the whole sample but affect significantly the local characteristics of the material,[12] (ii) large solubilities due to high external pressure, as it is believed to be the case in the Earth’s core,[7], and finally (iii) because an externally-driven tetragonal distortion of the lattice definitively favors the occupation of O-sites over T-sites. Furthermore, a tetragonal distortion of the required kind happens naturally along the pathway introduced by Bain to account for the phase transformation between bcc and fcc iron.[13] A self-sustained scenario can be realized here: the tetragonal distortion behind the phase transition favors the occupation of O-sites, and in turn, increasing the population at these sites drives the necessary distortion for the phase transformation. In this paper, we shall study the modification of kinetics barriers for a $\text{bcc} \rightarrow \text{fcc} \rightarrow \text{hcp}$ transformation due to the role of interstitials occupying O-sites.

The tetragonal distortion of the bcc lattice belongs to the group of martensitic transformations, which represent a diffusion-less, cooperative, homogeneous movement of the atoms providing a change in the crystal structure that can be monitored by symmetry operations, lattice distances and or unit cell volumes.[13, 14] Adsorbing hydrogen in O-sites deforms the bcc lattice into a body-centred-tetragonal (bct) phase (Fig. 1). [10] The tetragonal distortion consists of a contraction upon two of the cubic axes ($a = b$), while the third one expands (c). When the c/a ratio reaches the value $\sqrt{2}$ the bct lattice becomes face-centred-cubic (fcc), also known as γ -Fe, a stable frustrated antiferromagnetic phase of iron. According to our calculations, for values of $c/a \geq 1.5$ and a stoichiometry Fe_2H a further transformation to an hexagonal phase (ϵ -Fe) takes place ($\gamma = 90^\circ \rightarrow 60^\circ$; Fig. 1). Bain’s pathway is not the only transformation suggested in the literature to explain the phase diagram of iron, but it has a number of advantages for the purposes of this work, namely: (i) it retains at each step the highest possible crystal symmetry, (ii) it is simple, and (iii) it contains the lattice deformation expected for hydrogen occupation of O interstitials.

Theory. Ab initio calculations have been carried out in the framework of DFT and pseudo-potentials theory. [15, 16] Actual calculations have been performed with the CASTEP code. [17] The Born-Oppenheimer approximation is used; ions are considered classical objects moving under the forces created by electrons obeying Schrödinger equation. Ultrasoft pseu-

dopotentials are used to describe Fe and H, and wavefunctions are expanded in plane-waves with a cut-off energy of 375 eV. The generalized gradients approximation for the exchange and correlation potential due to Perdew, Burke and Ernzerhof [18] has been chosen, and spin-polarized bands are considered to account for magnetism. The accuracy of our calculations is determined by the quality of the pseudo-potential, the cut-off energy, and the density of the k-points mesh used in the irreducible part of the Brillouin zone (a Monkhorst-Pack mesh of 10x10x10 [19]). The choice of these values for our calculations is related to previous studies where conditions for good convergence on relevant properties of iron such as the lattice parameter, magnetization, or bulk modulus have been assessed [10]. Other convergence thresholds are: (i) variation in the total energy $\leq 10^{-5}$ eV/atom, (ii) maximum residual force ≤ 0.001 eV/Å, (iii) maximum change in any atom position ≤ 0.001 Å. All the parameters defining the unit cell (distances and angles) have been optimized in order to minimize the stress for each crystal system (cubic, tetragonal and hexagonal): local minima have been optimized so the maximal residual pressure on the unit cell is $P \leq 0.01$ GPa (such a low threshold is convenient to compute elastic constants around equilibrium configurations), while barriers have been optimized to a threshold below ≤ 0.1 GPa, affecting the energy ≤ 0.007 eV. Barriers between these points have been estimated by a constrained optimization procedure where the parameters a/c and γ are kept fixed to different values and all the remaining parameters (including magnetization) are freely optimized so the system can reach the nearest local minima (Fig. 2) .

Results. To understand the role of interstitial hydrogen we compare the energy landscape of Fe and Fe₂H for various crystal symmetries. At T=0 K and P=0 GPa, the global minimum for Fe corresponds to ferromagnetic (FM) bcc Fe ($c/a = 1$, $\gamma = 90^\circ$). Varying continuously the c/a ratio we find two metastable configurations, first for Fe fct ($c/a \approx 1.51$), and then for hcp ($c/a \geq 1.6$, $\gamma = 60^\circ$). Their magnetic configurations are respectively anti-ferromagnetic type I (AF) and non-magnetic (NM) (Fig. 2). We have computed structural parameters and elastic constants for these three configurations (upper sections in Tables I and II): there is an overall good agreement with the available experimental data and all the elastic constants are positive and consistent with the symmetry, proving that they are truly locally stable minima. We notice, however, that theory predicts a frustrated antiferromagnetic fct phase ($c/a \approx 1.5$), not a pure fcc cristal ($c/a = \sqrt{2}$) as it has been experimentally reported.[20] In agreement with other authors we remark the importance of magnetism to understand the

phase diagram of iron.[21–24] The contribution to the total energy of magnetism is itself small, but crucial since it is similar to differences between local minima and barriers (≤ 0.2 eV/unit cell). Furthermore, every important change in the magnetic state (from FM to AF, to NM) is accompanied by a corresponding sudden change in the unit cell volume: a decrease in the volume increases the overlap of electrons in the sp-like bands increasing the delocalization energy (kinetic) and reducing the strength of magnetism (Fig. 2a).

Interstitial hydrogen absorbed on the octahedral site has an important effect on the above picture. The internal pressure on the bcc lattice is approximately given by the stress tensor:

$$\sigma = \begin{bmatrix} 10 & 0 & 0 \\ 0 & 10 & 0 \\ 0 & 0 & -12 \end{bmatrix} (GPa)$$

It is obvious how this internal stress is responsible for the bct deformation of the unit cell that drives the system along the Bain’s pathway towards the fcc first, and subsequently to an hexagonal phase reached by a mere shear and a shuffle of the atoms in the unit cell.[25] We notice in passing that hydrostatic pressures between 10 and 20 GPa mark the onset of the transformation between the bcc and the hcp phases at low temperatures.[26] The internal pressure derived from the hydrogen presence is in the same range of values, therefore the behavior in Fig. 3, where barriers for the phase transformation have disappeared, is not at all surprising. During this transformation the magnetic interaction gets weaker in the region $c/a \approx 1.5 - 1.6$, and the volume of the unit cell is accordingly reduced by $\approx 15\%$. This is in good agreement with the experimental evidence for the ϵ -Fe phase, where it is known that hydrogen does not absorb in tetrahedral sites, and magnetism is weak.[27] In particular, the non-magnetic hexagonal structure for clean Fe ($c/a = 1.63$) is believed to exist at high pressure in the Earth’s core.[27] However, in the presence of interstitials we observe how the system is pushed further along the path to reach a sharp minimum at $c/a = 1.71$ ($\gamma = 60^\circ$), where the volume increases again and the ferromagnetism is restored in the material. Variations in the volume of the unit cell reflect the need of the system to minimize internal stresses, but these changes, now nearly twice the ones for clean iron, facilitate the appearance of defects in the material. Similarly to pristine iron, experimental and theoretical parameters in Tables I and II agree well, except for the predicted ferromagnetism for Fe_2H , that Antonov et al. did not find on the hexagonal phase of Fe_2D . [27]

Conclusions. Calculations for the Bain path of clean iron have allowed us to investigate the different stable/metastable phases of iron according to the energetic of the structures. Interstitial hydrogen hosted on O-sites becomes a source of large internal stress that can be released by a body-centered tetragonal deformation that fits naturally with Bain’s mechanism. DFT calculations show that the bcc phase is deformed until it reaches an AF-type I phase with $c/a = 1.5$ (close to the fcc crystal structure). It is favorable for the system to continue deforming to reach a paramagnetic minimum with hexagonal symmetry ($c/a = 1.6$ and $\gamma = 60^\circ$). This scenario agrees with current ideas about the Earth’s core composition under extreme external pressure. The internal pressure introduced by interstitial hydrogen can be thought as an effective temperature given to the system, and can be useful to understand the iron phase diagram. It is known that the γ to α transformation happens fast up to a critical temperature, M_s , but for higher temperatures it is slowed by competition with a different process. Our calculations show that such a martensitic transformation should compete with the formation of an ϵ phase favored by the accumulation of interstitials in octahedral sites. This process inhibits the γ to α phase transition because small nucleation seeds are formed that will grow by attracting further hydrogen diffusing fast at high temperatures.

Acknowledgments. This work has been financed by the Spanish MICINN (MAT2008-1497 and BIA2010-18863), and MEC (CSD2007-41 "NANOSELECT" and "SEDUREC").

-
- [1] N. Eliaz, A. Shachar, B. Tal, and D. Eliezer, Engineering Failure Analysis **9**, 167 (2002).
 - [2] Y. Liang, P. Sofronis, and N. Aravas, Acta Materialia **51**, 2717 (2003).
 - [3] Y. Tateyama and T. Ohno, Phys. Rev. B **67**, 174105 (2003).
 - [4] M. Elices, J. of Mat. Sci. **39**, 3889 (2004).
 - [5] J. Sanchez, J. Fullea, C. Andrade, and C. Alonso, Corrosion Science **49**, 4069 (2007).
 - [6] M. Dadfarnia, P. Novak, D. C. Ahn, J. B. Liu, P. Sofronis, D. D. Johnson, and I. M. Robertson, Advanced Materials **22**, 1128 (2010).
 - [7] D. Alfe, M. J. Gillan, and G. D. Price, J. Chem. Phys. **116**, 7127 (2002).
 - [8] E. I. Isaev, N. V. Skorodumova, R. Ahuja, Y. K. Vekilov, and B. Johansson, PNAS **104**, 9168 (2007).
 - [9] D. E. Jiang and E. A. Carter, Phys. Rev. B **70**, 064102 (2004).

- [10] J. Sanchez, J. Fullea, C. Andrade, and P. L. de Andres, Phys. Rev. B **78**, 014113 (2008).
- [11] J. Sanchez, J. Fullea, M. C. Andrade, and P. L. de Andres, Phys. Rev. B **81**, 132102 (2010).
- [12] M. Castellote, J. Fullea, P. G. de Viedma, C. Andrade, C. Alonso, I. Llorente, X. Turrillas, J. Campo, J. S. Schweitzer, T. Spillane, et al., N. Instr. and Methods in Phys. Research B **259**, 975 (2007).
- [13] E. C. Bain, Trans. Am. Inst. Min. Metall. Eng. **70**, 25 (1924).
- [14] V. L. Sliwko, P. Mohn, K. Schwarz, and P. Blaha, J. Phys.: Condens. Matter **8**, 799 (1996).
- [15] W. Kohn and L. J. Sham, Phys. Rev. **140**, A1133 (1964).
- [16] D. Vanderbilt, Phys. Rev. B **41**, 7892 (1990).
- [17] S. Clark, M. D. Segall, C. Pickard, P. Hasnip, M. J. Probert, K. Refson, and M. C. Payne, Z. fuer Kristallographie **220**, 567 (2005).
- [18] J. P. Perdew, K. Burke, and M. Ernzerhof, Phys. Rev. Lett. **77**, 3865 (1996).
- [19] H. J. Monkhorst and J. D. Pack, Phys. Rev. B **13**, 5188 (1976).
- [20] M. Acet, H. Zähres, E. F. Wassermann, and W. Pepperhoff, Phys. Rev. B **49**, 6012 (1994).
- [21] H. Hasegawa and D. G. Pettifor, Phys. Rev. Lett. **50**, 130 (1983).
- [22] G. L. Krasko and G. B. Olson, Phys. Rev. B **40**, 11536 (1989).
- [23] S. Tsurekawa, K. Okamoto, K. Kawahara, and T. Watanabe, J. Mater. Sci. **40**, 895 (2005).
- [24] S. V. Okatov, A. R. Kuznetsov, Y. N. Gornostyrev, V. N. Urtsev, and M. I. Katsnelson, Phys. Rev. B **79**, 094111 (2009).
- [25] K. J. Caspersen, A. Lew, M. Ortiz, and E. A. Carter, Phys. Rev. Lett. **93**, 115501 (2004).
- [26] A. P. Jephcoat, H. K. Mao, and P. M. Bell, J. Geophys. Res. **91**, 4677 (1986).
- [27] V. E. Antonov, K. Cornell, V. K. Fedotov, A. I. Kolesnikov, E. G. Ponyatovsky, V. I. Shiryaev, and H. Wipi, J. of Alloys and Compounds **264**, 214 (1998).
- [28] C. Kittel, *Introduction to Solid State Physics* (Wiley, 8th ed., New York, 2005).
- [29] J. Zarestky and C. Stassis, Phys. Rev. B **35**, 4500 (1987).
- [30] A. K. Singh, H.-k. Mao, J. Shu, and R. J. Hemley, Phys. Rev. Lett. **80**, 2157 (1998).

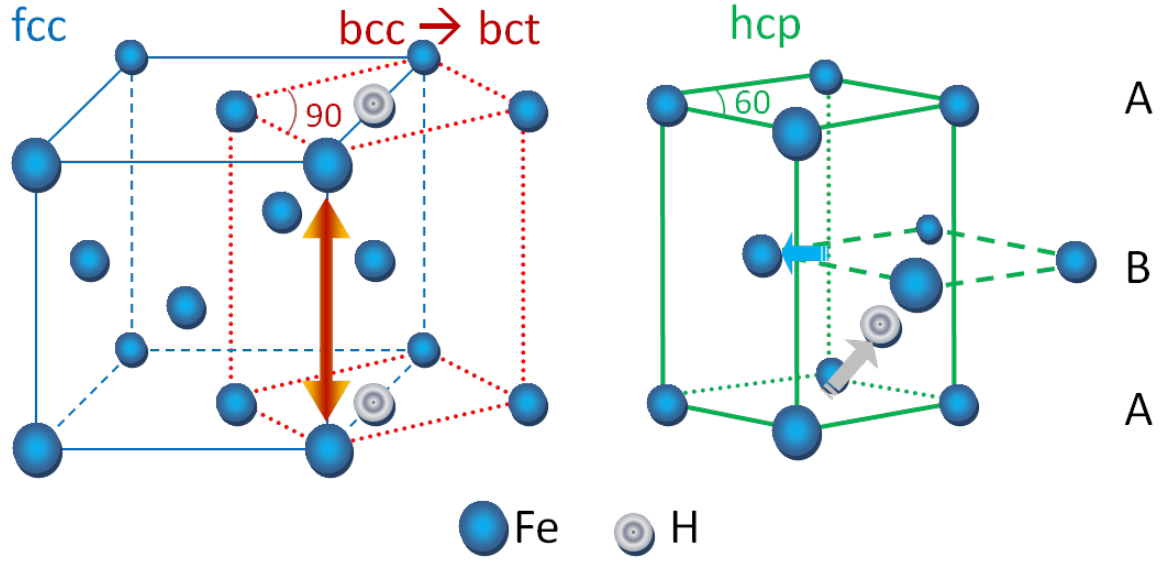


FIG. 1: (color online) Unit cell sketch along Bain's transformation: bcc ($c/a = 1$, middle), fcc ($c/a = \sqrt{2}$, left), hcp ($c/a = 1.6$, right). The Octahedral high symmetry site (O) is shown as grey circle.

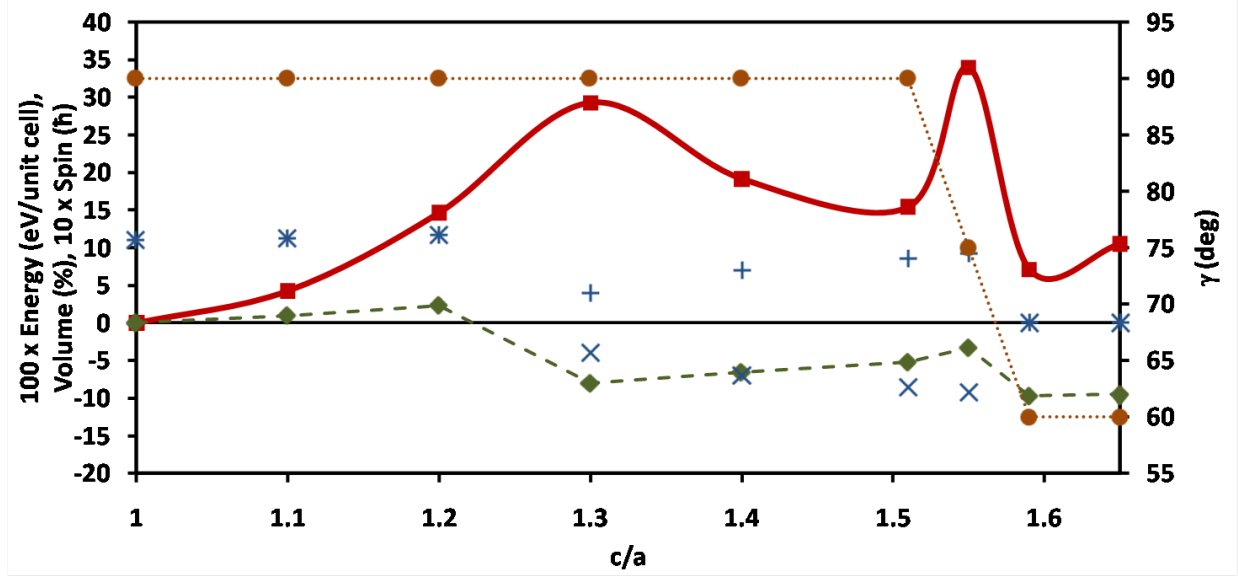


FIG. 2: (color online) Along Bain's pathway represented in Fig. 1 (from $c/a = 1$ –cubic– to $c/a = 1.6$ –hexagonal–): (i) γ in degrees (right y-axis, brown dotted line and circles), (ii) enthalpy in eV/unit cell (left y-axis, red thick continuous line and squares; to increase visibility values have been multiplied by an arbitrary factor of 100); (iii) volume of the unit cell expressed as the fractional variation with respect to the global minimum value at $c/a = 1$ (right y-axis, green dashed line and diamonds), (iv) spin population in \hbar on the two iron atoms in the unit cell: Fe(1) and Fe(2) (left y-axis, blue + and \times respectively; to increase visibility the numerical value has been multiplied by an arbitrary factor of 10). Notice how the transformation between ferromagnetic (both spins are positive) to antiferromagnetic (spins have opposite signs) to non-magnetic (both are zero) are related to sudden variations in the volume of the unit cell. Lines joining symbols have been drawn to guide the eye only.

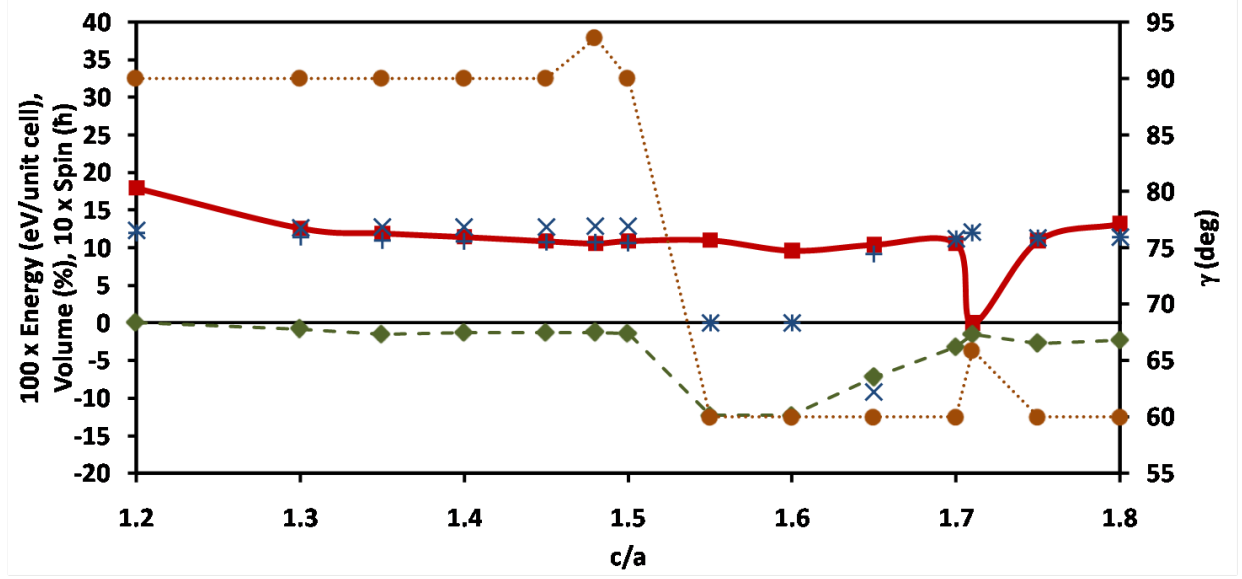


FIG. 3: (color online) For Fe₂H, same as caption in Fig. 2.

TABLE I: For the different phases of clean iron (above) and Fe_2H (below) theoretical and experimental parameters: IT is the number of the symmetry group in the International Tables for Crystallography, lattice parameter a is given in Å and the unit cell volume in Å³, enthalpies in eV, forces in eV/atom, spin in μ_B , and Bulk modulus in GPa. Notice that for Fe_2H , the FM and NM hcp are quasi-degenerated in energy, with FM the slightly more stable configuration at T=0 K. The fct-AF* phase corresponds to a tetragonal distortion of the fcc ($c/a = 1.5$) with a frustrated anti-ferro configuration.

SYSTEM	IT	a (Å)	c/a	s (μ_B)	vol Å ³	B (GPa)
Fe						
BCC	229	2.82	1.00	2.2	22.33	210
BCC[28]	229	2.87	1.00	2.2	22.80	172
FCT	139	2.43	1.50	0.0	20.27	207
FCC[29]	225	2.55	1.42	0.0	23.55	133
HCP	194	2.45	1.58	0.0	22.16	311
HCP[26]	194	2.58	1.62	0.0	24.09	180
Fe_2H						
MONOCLINIC	12	2.53	1.71	2.39	24.85	183
HCP[27]	194	2.58	1.62	0.0	24.09	-

TABLE II: Elastic constants (GPa) computed at the relevant local minima for Fe and Fe₂H (upper and lower, respectively).

	C_{11}	C_{12}	C_{13}	C_{33}	C_{44}	C_{55}	C_{66}
<hr/>							
Fe							
<hr/>							
TH bcc FM	305	162			121		
EXP bcc FM[30]	281	144			123		
TH fct AF*	579	120	265	10	196		50
EXP fcc[29]	154	122			77		
TH hcp NM	570	187	158	661	184		191
EXP hcp NM[30]	640	300	254	648	422		
<hr/>							
Fe ₂ H							
<hr/>							
monoclinic, FM	322	124	97	329	104	73	104
<hr/>							